MVDR Beam Patterns of an Acoustic Vector Hydrophone Located Near a Reflecting Boundary

Mahmood Padash[1], Hengameh Keshavarz[2], javad ahmadi shokouh[3] and Farahnaz mohanna[4]
1- Faculty of Electrical and Computer Engineering, University of Sistan and Baluchestan, Zahedan, Iran.
Email: mf.padash@gmail.com
2, 3, 4- Faculty of Electrical and Computer Engineering, University of Sistan and Baluchestan, Zahedan, Iran.
Email: hkeshavarz@ieee.org

Received X X X Revised X X X Accepted X X X

ABSTRACT:
A vector hydrophone is composed of two or three spatially collocated but orthogonally oriented velocity hydrophones plus an optional collocated pressure hydrophone. A vector hydrophone may form azimuth-elevation beams that are invariant with respect to the sources' frequencies, bandwidths and radial locations. This paper characterizes the minimum variance distortionless response (MVDR) beam patterns associated with a single underwater acoustic vector hydrophone located near a reflecting boundary for the far-field underwater acoustic sources.

KEYWORDS: Beam Pattern, MVDR Beamformer, vector hydrophone, Near a Reflecting Boundary

1. INTRODUCTION

A vector hydrophone consists of two or three identical, co-located, but orthogonally oriented velocity hydrophones plus another co-located pressure hydrophone. Each velocity hydrophone measures one Cartesian component of the three-dimensional particle velocity wave field. On the other hand, a pressure hydrophone measures the acoustical pressure as a scalar entity. Therefore, a single-vector hydrophone thus has a two-dimensional (2-D) azimuth-elevation directivity that is independent of signal frequency, signal bandwidth, and the source's location.

A receiving sensor array beamformer spatially filters the received data to separate the desired signals from interferences and noise based on any difference between their directions of arrival. A receiving beamformer may be further classified as data-independent or data-dependent [7].One data-dependent beamformer is the MVDR beamformer [7], which preserves the desired signal's energy but exploits interference and noise information embedded in the received data to minimize the beamformer output's interference plus noise variance. In so doing, it is statistically optimum in that it maximizes its output signal-to-interference-plus-noise ratio (SINR).

The measurement models of a vector hydrophone located way from and near a reflecting boundary are developed and introduced to the signal processing research community, respectively, by [1] and [12]. The use of the vector hydrophone for sensor array direction finding away from a reflecting boundary has been investigated in [2]-[6] and [8]-[11]. [13] Presents the spatial matched filter beam patterns and the minimum variance distortionless response (MVDR) beam patterns associated with the vector hydrophone located away from any reflecting boundary. Then, [14] presents the spatial matched filter beam patterns, when a single vector hydrophone located near a reflecting boundary. Up to now, MVDR beam patterns of the vector hydrophone located near a reflecting boundary has not been investigated in the literature.

In this paper, the MVDR beam patterns of the acoustic vector hydrophone located near a reflecting boundary for the far-field underwater acoustic sources is presented.

This paper is organized as follows: Section II introduces the array manifold of the vector hydrophone located near a reflecting boundary. In section III, the MVDR beam patterns of the vector hydrophone is investigated. Section IV presents experimental results and discussion. Finally, the results are summarized and concluded in section V.

2. THE ARRAY MANIFOLD OF AN ACOUSTIC VECTOR HYDROPHON LOCATED NEAR A REFLECTING BOUNDARY

Construction #1: the array manifold of an acoustic vector hydrophone derived and introduced respectively by [12]. Four-component vector-hydrophone (consists of three orthogonally oriented velocity hydrophones aligned along the x, y and z axes, plus a pressure hydrophone) gives an array manifold

$$\boldsymbol{a}_k^{(x+y+z+p)}(\psi_k,\varphi_k)=\begin{bmatrix}\left(1+R(\psi_k)e^{-j\alpha_k}\right)cos(\psi_k)cos(\varphi_k)\\ \left(1+R(\psi_k)e^{-j\alpha_k}\right)cos(\psi_k)sin(\varphi_k)\\ \left(1-R(\psi_k)e^{-j\alpha_k}\right)sin(\psi_k)\\ \left(1+R(\psi_k)e^{-j\alpha_k}\right)\end{bmatrix} \quad (1)$$

Where $0 \le \psi_k \le \pi/2$ denotes the κth source's elevation angle measured from the X-Y plan, $0 \le \varphi_k \le 2\pi$ refers the κth source's azimuth angle measured from the positive X axes, λ symbolizes the wavelength, and $\alpha_k \overset{def}{=} \frac{4\pi D}{\lambda} sin(\psi_k)$.

The reflecting boundary, herein assumed to be a two-dimensional Cartesian plane of infinite size, is situated at $Z = -D$ and the vector hydrophone is located at the origin of the Cartesian coordinates. The reflection coefficient, $R(\psi_k)$ expresses the attenuation and phase change of the reflected planewave. It is generally a function of both frequency and incidence angle. Under such condition that derived by [12], the rigid boundary condition occurs whenever the reflecting surface reflecting boundary is not acoustically pliable, mathematically, the condition is expressed by $R = 1$ for all incidence angles. In contrast, the pressure-release boundary condition occurs whenever the surface or reflecting boundary is highly acoustically pliable, In this case $R = -1$ for all incidence angles. Finally, with substitute $R = 0$ in (1), the array manifold of an acoustic vector hydrophone located away from a reflecting boundary is appearing.

Construction #2: Three-component vector-hydrophone (consists of three orthogonally oriented velocity hydrophones aligned along the x, y and z axes) gives an array manifold

$$\boldsymbol{a}_k^{(x+y+z)}(\psi_k,\varphi_k)=\begin{bmatrix}\left(1+R(\psi_k)e^{-j\alpha_k}\right)cos(\psi_k)cos(\varphi_k)\\ \left(1+R(\psi_k)e^{-j\alpha_k}\right)cos(\psi_k)sin(\varphi_k)\\ \left(1-R(\psi_k)e^{-j\alpha_k}\right)sin(\psi_k)\end{bmatrix} \quad (2)$$

Construction #3: Three-component vector hydrophone (consists of two orthogonally oriented velocity hydrophones aligned along the x and y axes, plus a pressure hydrophone) gives an array manifold

$$\boldsymbol{a}_k^{(x+y+p)}(\psi_k,\varphi_k)=\begin{bmatrix}\left(1+R(\psi_k)e^{-j\alpha_k}\right)cos(\psi_k)cos(\varphi_k)\\ \left(1+R(\psi_k)e^{-j\alpha_k}\right)cos(\psi_k)sin(\varphi_k)\\ \left(1+R(\psi_k)e^{-j\alpha_k}\right)\end{bmatrix} \quad (3)$$

Construction #4: Three-component vector hydrophone (consists of two orthogonally oriented velocity hydrophones aligned along the x and y axes) gives an array manifold

$$\boldsymbol{a}_k^{(x+y)}(\psi_k,\varphi_k)=\begin{bmatrix}\left(1+R(\psi_k)e^{-j\alpha_k}\right)cos(\psi_k)cos(\varphi_k)\\ \left(1+R(\psi_k)e^{-j\alpha_k}\right)cos(\psi_k)sin(\varphi_k)\end{bmatrix} \quad (4)$$

3. MVDR BEAMFORMING WITH A VECTOR HYDROPHONE

The MVDR beamformer is a data-dependent beamformer which preserves the desired signal's energy but exploits interference and noise information embedded in the received data to minimize the beamformer output's interference-plus-noise variance.

In this paper, like [13] assume that exist a zero spatio-temporal cross correlation between the desired signal, interferers, and the additive noise. Furthermore, the additive noise is zero-mean and spatio–temporally uncorrelated but may have unequal variance across the component hydrophones.

The MVDR beamformer output's SINR with only a single interferer equals

$$SINR^{max} = p_s\left(\left\|\tilde{\boldsymbol{a}}_s\right\|^2 + \frac{p_i\left|\tilde{\boldsymbol{a}}_s^H\tilde{\boldsymbol{a}}_i\right|^2}{1+p_i\left\|\tilde{\boldsymbol{a}}_i\right\|^2}\right) \quad (5)$$

Where the superscript H denotes complex conjugate transpose, p_s denotes the desired signal's power, p_i refers to the interferer's power, $\tilde{\boldsymbol{a}}_i \overset{def}{=} \boldsymbol{P}_n^{-1/2}\boldsymbol{a}_i$,

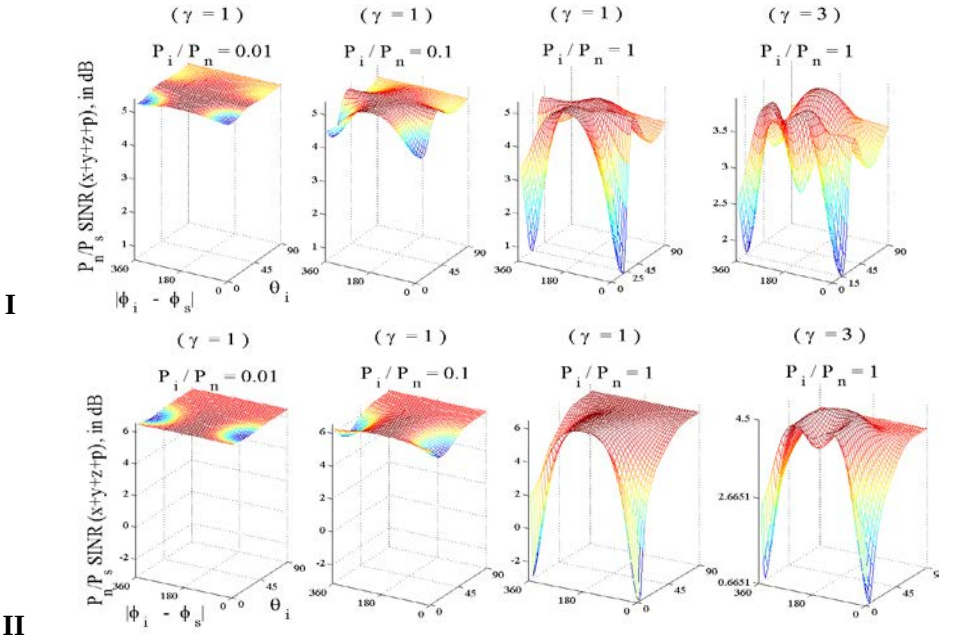

Fig. 1. MVDR beam patterns of construction #1 for $D/\lambda = 0.5$, $\psi_s = 45^\circ$ and $\gamma = 1$ for the equal-noise-variance case, $\gamma = 3$ for the unequal-noise-variance case, **I**) rigid boundary and **II**) pressure release boundary.

$\tilde{\boldsymbol{a}}_s \overset{def}{=} \boldsymbol{P}_n^{-1/2}\boldsymbol{a}_s$, $\boldsymbol{P}_n$ symbolizes the additive noise's spatial covariance matrix, $\boldsymbol{a}_s$ represents the desired signal's steering vector, $\boldsymbol{a}_i$ refers to the interferer's steering vector. And, $\left(\boldsymbol{P}_n^{-1/2}\right)^H = \boldsymbol{P}_n^{-1/2}$.

The following analysis will focus on the case where the noise variance equals p_n for all velocity hydrophones but γp_n for the pressure hydrophone (if present). However, in the case where the noise variance p_n equals across all component hydrophones $\gamma = 1$.

Construction #1:

Additive noise's spatial covariance matrix equals

$$\boldsymbol{P}_n \overset{def}{=} p_n \begin{bmatrix} 1 & & & \\ & 1 & & \\ & & 1 & \\ & & & \gamma \end{bmatrix} \tag{6}$$

And

$$\left\|\tilde{\boldsymbol{a}}_s^{(x+y+z+p)}\right\|^2 = \frac{2 + 1/\gamma + 2R\cos\alpha_s\left(1/\gamma + \cos 2\psi_s\right)}{p_n}$$

$$\left\|\tilde{\boldsymbol{a}}_i^{(x+y+z+p)}\right\|^2 = \frac{2 + 1/\gamma + 2R\cos\alpha_i\left(1/\gamma + \cos 2\psi_i\right)}{p_n}$$

$$\left|\left(\tilde{\boldsymbol{a}}_s^{(x+y+z+p)}\right)^H \tilde{\boldsymbol{a}}_i^{(x+y+z+p)}\right|^2 = \frac{\left(E\left[1/\gamma + A\right] + GB\right)^2 + \left(F\left[1/\gamma + A\right] + HB\right)^2}{p_n^2}$$

Where,

$$A = \cos\psi_s \cos\psi_i \cos\left(\varphi_i - \varphi_s\right) \quad , \quad B = \sin\psi_s \sin\psi_i$$

$$E + jF = \left[R e^{j\alpha_s} + 1\right]\left[R e^{-j\alpha_s} + 1\right]$$

$$G + jH = \left[R e^{j\alpha_s} - 1\right]\left[R e^{-j\alpha_s} - 1\right]$$

$$\alpha_s = \frac{4\pi D}{\lambda}\sin\psi_s \quad , \quad \alpha_i = \frac{4\pi D}{\lambda}\sin\psi_i$$

Hence,

$$SINR_{max}^{(x+y+z+p)} = \frac{p_s}{p_n}\left(2 + 2/\gamma + 2R\cos\alpha_s\left[1/\gamma + \cos 2\psi_s\right]\right) - \frac{\frac{p_i}{p_n}\left(\left[E\left(1/\gamma + A\right) + GB\right]^2 + \left[F\left(1/\gamma + A\right) + HB\right]^2\right)}{1 + \frac{p_i}{p_n}\left(2 + 2/\gamma + 2R\cos\alpha_i\left[1/\gamma + \cos 2\psi_i\right]\right)} \tag{7}$$

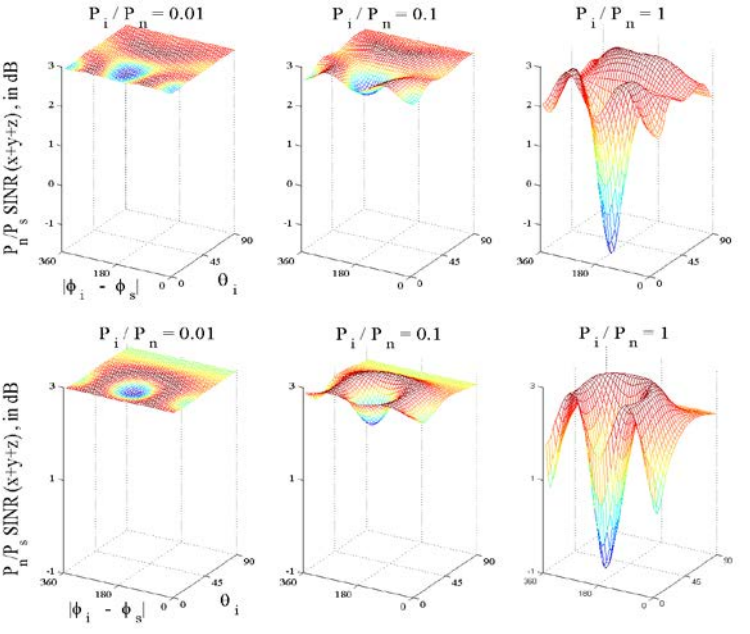

Fig. 2. MVDR beam patterns of construction #2 for $D/\lambda = 0.5$, $\psi_s = 45^\circ$ and $\gamma = 1$, **I**) rigid boundary and **II**) pressure release boundary

Construction #2:

$$\left\| \tilde{\boldsymbol{a}}_s^{(x+y+z)} \right\|^2 = \frac{2 + 2R\cos\alpha_s \cos 2\psi_s}{p_n}$$

$$\left\| \tilde{\boldsymbol{a}}_i^{(x+y+z)} \right\|^2 = \frac{2 + 2R\cos\alpha_i \cos 2\psi_i}{p_n}$$

$$\left| \tilde{\boldsymbol{a}}_s^{(x+y+z)H} \tilde{\boldsymbol{a}}_i^{(x+y+z)} \right|^2 = \frac{[EA + GB]^2 + [FA + HB]^2}{p_n^2}$$

Hence,

$$SINR_{max}^{(x+y+z)} = p_s/p_n \left[\frac{(2 + 2R\cos\alpha_s\cos 2\psi_s) - \frac{p_i}{p_n}\left([EA+GB]^2 + [FA+HB]^2\right)}{1 + \frac{p_i}{p_n}(2 + 2R\cos\alpha_i\cos 2\psi_i)} \right] \quad (8)$$

Construction #3:

Additive noise's spatial covariance matrix equals

$$\boldsymbol{P}_n \overset{def}{=} p_n \begin{bmatrix} 1 & & \\ & 1 & \\ & & \gamma \end{bmatrix} \quad (9)$$

$$\left\| \tilde{\boldsymbol{a}}_s^{(x+y+p)} \right\|^2 = \frac{[2 + 2R\cos\alpha_s]\left[1/\gamma + \cos^2\psi_s\right]}{p_n}$$

$$\left\| \tilde{\boldsymbol{a}}_i^{(x+y+p)} \right\|^2 = \frac{[2 + 2R\cos\alpha_i]\left[1/\gamma + \cos^2\psi_i\right]}{p_n}$$

$$\left| \tilde{\boldsymbol{a}}_s^{(x+y+p)H} \tilde{\boldsymbol{a}}_i^{(x+y+p)} \right|^2 = \frac{\left[E\left(1/\gamma + A\right)\right]^2 + \left[F\left(1/\gamma + A\right)\right]^2}{p_n^2}$$

Hence,

$$SINR_{max}^{(x+y+p)} = p_s/p_n \left[\frac{(2 + 2R\cos\alpha_s)\left(1/\gamma + \cos^2\psi_s\right) - \frac{p_i}{p_n}\left(\left[E\left(1/\gamma + A\right)\right]^2 + \left[F\left(1/\gamma + A\right)\right]^2\right)}{1 + \frac{p_i}{p_n}(2 + 2R\cos\alpha_i)\left(1/\gamma + \cos^2\psi_i\right)} \right] \quad (10)$$

Construction #4:

$$\left\| \tilde{\boldsymbol{a}}_s^{(x+y)} \right\|^2 = \frac{\left[2 + 2R\cos\alpha_s\right]\cos^2\psi_s}{p_n}$$

$$\left\| \tilde{\boldsymbol{a}}_i^{(x+y)} \right\|^2 = \frac{\left[2 + 2R\cos\alpha_i\right]\cos^2\psi_i}{p_n}$$

$$\left| \tilde{\boldsymbol{a}}_s^{(x+y)H} \tilde{\boldsymbol{a}}_i^{(x+y)} \right|^2 = \frac{[EA]^2 + [FA]^2}{p_n^2}$$

$$SINR_{max}^{(x+y)} = p_s/p_n \left[\frac{(2 + 2R\cos\alpha_s\cos^2\psi_s) - \frac{p_i}{p_n}\left([EA]^2 + [FA]^2\right)}{1 + \frac{p_i}{p_n}(2 + 2R\cos\alpha_i)\cos^2\psi_i} \right] \quad (11)$$

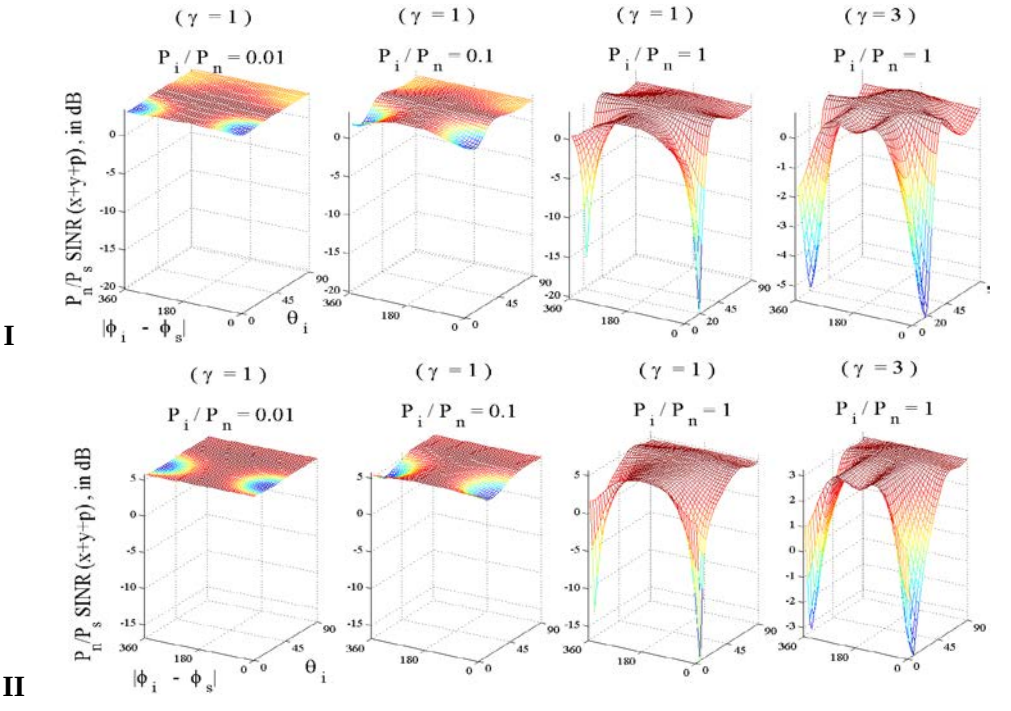

Fig. 3. MVDR beam patterns of construction #3 for $D/\lambda = 0.5$, $\psi_s = 45^\circ$ and $\gamma = 1$ the equal-noise-variance case, $\gamma = 3$ for the unequal-noise-variance case, **I**) rigid boundary and **II**) pressure release boundary

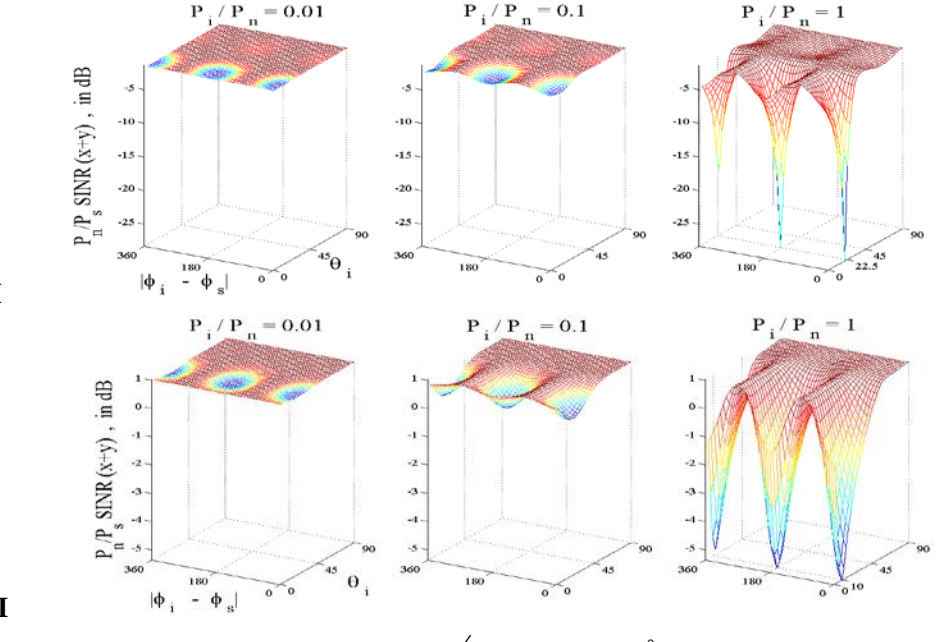

Fig. 4. MVDR beam patterns of construction #4 for $D/\lambda = 0.5$, $\psi_s = 45^\circ$ and $\gamma = 1$, **I**) rigid boundary and **II**) pressure release boundary.

4. NUMERICAL RESULTS AND DISCUSSION

Figure 1 shows MVDR beam patterns for construction #1 in the presence of a rigid or a pressure-release reflecting boundary for $D/\lambda = 0.5$, $\psi_s = 45^\circ$.

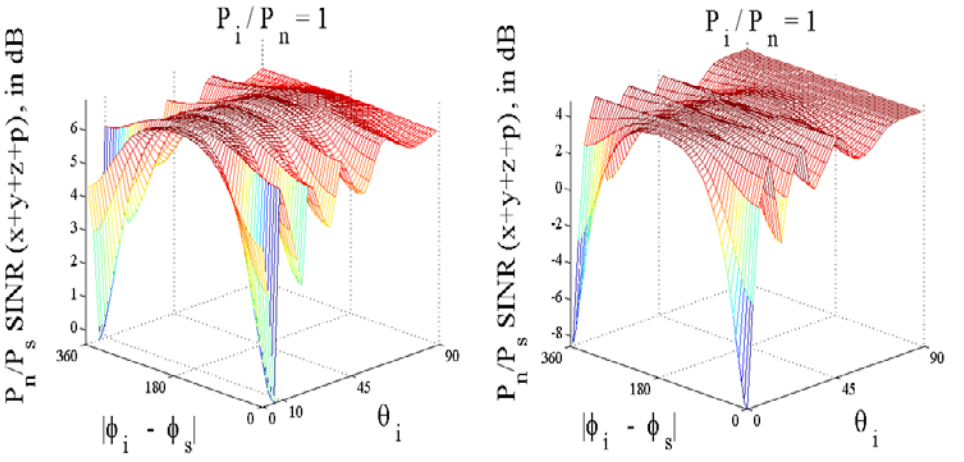

Fig. 5. MVDR beam patterns of construction #1 for $D/\lambda = 2$, $\psi_s = 45^\circ$ and $\gamma = 1$, **(a)** rigid boundary and **(b)** pressure release boundary

As this figure indicates, $p_n/p_s\ SINR^{(x+y+z+p)}_{max}$ have two minima at $|\varphi_i - \varphi_s| = \{0°, 360°\}$ (when the desired source and the interference impinge from the same azimuth angles). In contrast, there is difference between the interference's elevation angle (ψ_i) and the desired source's elevation angle ($\psi_s = 45^\circ$). These two minima appear when $\frac{p_i}{p_n}$ or INR equal to or greater than unity.

The right side of Fig. 1 plots the unequal variance case with ($\gamma = 3$) for both rigid and pressure release boundary. An increase in γ causes an unique minimum at $|\varphi_i - \varphi_s| = 180^\circ$, although it is not a very signify-cant event at least for the pressure release reflecting boundary. As this figure shows, the change in γ also affects the overall level of $p_n/p_s\ SINR^{(x+y+z+p)}_{max}$.

Like Figure 1, Figure 2 shows MVDR beam patterns, but for construction #2. As this figure indicates, $p_n/p_s\ SINR^{(x+y+z)}_{max}$ is minimum at $|\varphi_i - \varphi_s| = 180^\circ$, and have two local minima at $|\varphi_i - \varphi_s| = \{0°, 360°\}$ (when the desired source and the interference impinge from the same azimuth angles). The difference between results in Fig. 1 and Fig. 2 is caused by pressure hydrophone (with or without a pressure hydrophone). Like Figures 1 and 2, Figure 3 and Figure 4 Similarly indicate same results respectively for construction #3 (with a pressure hydrophone and without z-axes velocity hydrophone) and construction #4 (without the pressure hydrophone and z-axes velocity hydrophone).

Figure 5 shows that increasing D/λ from 0.5 to 2 causes periodic local minimums for construction #1 in the presence of a rigid or a pressure release reflecting boundary. The period of the peaks depends on the value of D/λ . The more D/λ increases, the more the period of the local minimums decreases. Similarly, increasing D/λ leads to more minimums for the other constructions.

5. CONCLUSION

In this paper, the MVDR beam patterns of the vector hydrophone located near an infinite-size reflecting boundary for the far-field underwater acoustic sources have been investigated for different constructions. Increasing γ appears local minimum and a slight dent in edges, also decreases the overall level of SINR. In constructions of a vector hydrophone that not consist of a pressure hydrophone, SINR has a minimum at $|\varphi_i - \varphi_s| = 180^\circ$, when the desired source and the interference imping from the diametrically opposite azimuth angels. Increasing D/λ produces more local minimums in the beam patterns. Furthermore, the local minimums are repeated periodically with respect to ψ_i and the period depends on the value of D/λ .

The pressure hydrophone's presence avoids spurious beamforming peaks. The vertical velocity hydrophone's presence aid beamforming toward

vertical incident angles. The omission of vertical velocity hydrophones can reduce vertically incident interference, but may introduce spurious beamforming peaks under some special scenarios. Thus, offers maximum azimuth-elevation beamforming maneuverability free of spurious peaks, but at the cost of greater hardware complexity. However, if the desired sources' incident angles area priori known to be near horizontal directions and the interference from near-vertical directions, then offers a simpler alternative with increased interference capability.

REFERENCES

[1] A. Nehorai and E. Paldi, **"Acoustic vector sensor array processing,"** *IEEE Trans. Signal Processing*, vol. 42, pp. 2481–2491, Sept. 1994.

[2] B. Hochwald and A. Nehorai, **"Identifiability in array processing models with vector-sensor applications,"** *IEEE Trans. Signal Processing*, vol. 44, pp. 83–95, Jan. 1996.

[3] M. J. Berliner and J. F. Lindberg, Acoustic Particle Velocity Sensors: Design, Performance and Applications. Woodbury, NY*:* AIP Press, 1996.

[4] B. A. Cray and A. H. Nuttall, **"A comparison of vector-sensing and scalar-sensing linear arrays,"** Naval Undersea Warfare Center Division, Newport, RI, NUWC-NPT Technical Report no. 10 632, Jan. 1997.

[5] K. T. Wong and M. D. Zoltowski, **"Closed-form underwater acoustic direction-finding with arbitrarily spaced vector-hydrophones at unknown locations,"** *IEEE J. Oceanic Eng.*, vol. 22, pp. 566–575, July 1997.

[6] K. T. Wong and M. D. Zoltowski, **"Extended-aperture underwater acoustic multisource azimuth/elevation direction-finding using uniformly but sparsely spaced vector hydrophones,"** *IEEE J. Oceanic Eng.*, vol. 22, pp. 659–672, Oct. 1997..

[7] B. D. Van Veen and K. M. Buckley, **"Beamforming: A versatile approach to spatial filtering,"** *IEEE Acoust., Speech Signal Processing Magazine*, pp. 4–24, Apr. 1988.

[8] M. Hawkes and A. Nehorai, **"Effects of sensor placement on acoustic vector-sensor array performance,"** *IEEE J. Ocean. Eng.*, vol. 24, pp. 33–40, Jan. 1999.

[9] K. T. Wong, **"Adaptive source localization and blind beamforming for underwater acoustic wideband fast frequency-hop signals of unknown hop sequences and unknown arrival angles using a vector-hydrophone,"** *in IEEE Wireless Communications & Networking Conf.*, vol. 2, 1999, pp. 664–668.

[10] K. T. Wong and M. D. Zoltowski, **"Root-MUSIC-based azimuth-elevation angle-of-arrival estimation with uniformly spaced but arbitrarily oriented velocity hydrophones,"** *IEEE Trans. Signal Processing*, pp. 3250–3260, Dec. 1999.

[11] K. T. Wong and M. D. Zoltowski, **"Self-initiating MUSIC-based direction finding in underwater acoustic particle velocity-field beamspace,"** *IEEE J. Oceanic Eng.*, vol. 25, pp. 262–273, Apr. 2000.

[12] M. Hawkes and A. Nehorai, **"Acoustic vector-sensor processing in the presence of a reflecting boundary,"** *IEEE Trans. Signal Processing*, vol. 48, pp. 2981–2993, Nov. 2000.

[13] K. T. Wong and H. Chi, **"Beam Patterns of an Underwater Acoustic Vector Hydrophone Located Away from any Reflecting Boundary,"** *IEEE Journal of Oceanic Engineering*, vol. 27, no. 3, pp. 628-637. July 2002.

[14] H. Keshavarz, **"Beam Patterns of an Underwater Acoustic Vector Hydrophone Located Near a Reflecting Boundary,"** *IEEE Oceans Conference*, pp. 585-588, 2004.